Promoting quantum correlations in deterministic quantum computation with a one-qubit model via postselection

Elisa I. Goettems,[1] Thiago O. Maciel,[1] Diogo O. Soares-Pinto,[2] and E. I. Duzzioni[1]
[1]*Departamento de Física, Universidade Federal de Santa Catarina, Florianópolis, SC, 88040-900, Brazil*
[2]*Instituto de Física de São Carlos, Universidade de São Paulo CP 369, 13560-970, São Carlos, São Paulo, Brazil*

(Received 15 November 2020; accepted 22 March 2021; published 19 April 2021)

The deterministic quantum computation with one qubit (DQC1) model is a restricted model of quantum computing able to calculate efficiently the normalized trace of a unitary matrix. In this work, we analyze the quantum correlations called entanglement, Bell's nonlocality, quantum discord, and coherence generated by the DQC1 circuit considering only two qubits (auxiliary and control). For the standard DQC1 model, only quantum discord and coherence appear. By introducing a filter in the circuit we purify the auxiliary qubit, taking it out from the totally mixed state and consequently promoting other quantum correlations between the qubits, such as entanglement and Bell's nonlocality. Through the optimization of the purification process, we conclude that even a small purification is enough to generate entanglement and Bell's nonlocality. We obtain, that by applying the purification process repeatedly an average of 12 times, the auxiliary qubit becomes 99% pure. In this situation, almost maximally entangled states are achieved, which almost maximally violate Bell's inequality. This result suggests that with a simple modification, the DQC1 model can be promoted to a universal model of quantum computing.

DOI: 10.1103/PhysRevA.103.042416

I. INTRODUCTION

As quantum correlations are exclusive to the quantum realm, we may expect that the advantages in processing, storing, and transmitting information are somehow connected to them. In the case of processing information, to have a speedup in relation to classical algorithms, quantum computing with pure states requires entanglement [1,2]. However, this requirement is not clear for quantum computation with mixed states. For instance, the deterministic quantum computation with one qubit (DQC1) [3] is a restricted model of quantum computing using a simple setup of a single pure qubit and n others in the totally mixed one. This simple scheme can evaluate the normalized trace of an arbitrary unitary matrix measuring just the first qubit. In Ref. [4], Datta *et al.* showed that this model requires little or null entanglement to perform the task of trace evaluation, suggesting a different quantum resource to explain the resulting computational gain [5], e.g., quantum discord [6]. Such an implication carries some ubiquity in physical models since the set of zero-discord states has zero measure and is nowhere dense, as shown in Ref. [7], which means that general quantum correlations beyond entanglement can be seen as a possible relevant resource for nonclassical characteristics. Notwithstanding, in Ref. [8] Dakić *et al.* presented a class of unitary matrices with null quantum discord without losing the quantum advantage. Continuing this investigation, the coherence of the control qubit was pointed out as the resource responsible for the speedup, given that it can be converted into other correlations [9,10].

The goal of this work is to promote quantum correlations in the DQC1 model. Because in the standard DQC1 model only quantum discord and coherence are present for two qubits, we use postselection to purify the auxiliary qubit such that entanglement and Bell's nonlocality are created.

This article is divided as follows: In Sec. II, we introduce the DQC1 circuit and the quantum correlation measures. The postselection process and the analysis of the results are given in Sec. III. Finally, our conclusions are described in Sec. IV.

II. QUANTUM CORRELATIONS IN THE STANDARD DQC1 MODEL

Introduced by Knill and Laflamme [3], the deterministic quantum computation with one qubit (DQC1) is a computing model that evaluates the normalized trace of any unitary operator using a measurement in a single qubit. The DQC1 circuit (see Fig. 1) consists of a control qubit in the state

$$\rho_0(\alpha) = \frac{(I + \alpha\sigma_Z)}{2},$$

where σ_Z is the Pauli matrix Z, a certain degree of coherence controlled by α ($0 \leqslant \alpha \leqslant 1$) and n auxiliary qubits initially in the totally mixed state,

$$\rho_n = \frac{I^{\otimes n}}{2^n},$$

where I is the identity operator.

In addition to the Hadamard gates,

$$H = \frac{1}{\sqrt{2}}\begin{bmatrix} 1 & 1 \\ 1 & -1 \end{bmatrix},$$

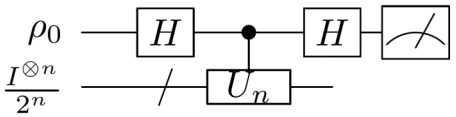

FIG. 1. DQC1 circuit used to evaluate the normalized trace of a unitary matrix U_n. The control qubit starts in a semipure state, $\rho_0(\alpha) = \frac{(I+\alpha\sigma_Z)}{2}$, with $0 \leqslant \alpha \leqslant 1$, while the n auxiliary qubits are in the maximum mixture state, $\rho_n = \frac{I^{\otimes n}}{2^n}$.

applied on the first qubit, the computation is performed by a controlled unitary between the first and auxiliary qubits. The result is obtained by measuring the expected values of the operators associated with the control qubit, whose precision is independent of the dimension of the unitary transformation U_n and depends only on the number of runs of the quantum circuit [4]. In contrast, the simplest classical algorithm to calculate the trace of a matrix depends on its dimension, which one can increase exponentially according to the number of qubits in the system [11].

With this advantage in mind, the idea is to map certain problems into the DQC1 model. Despite not being a universal model of quantum computing, some quantum solutions obtained through this model present advantages in comparison to their classical counterparts, such as spectral density estimation [3], testing integrability [12], Shor factorization [13], evaluation of average fidelity decay [14], estimate of Jones polynomials [15], and quantum metrology [16,17]. Inspired by these results, some experimental implementations of this model have been made in optical [18,19], nuclear magnetic resonance [20,21], superconducting materials [22], and cold atoms [23].

A. Quantum correlations in the DQC1 model

We start by writing the output state of the DQC1 circuit for two qubits in the Fano representation [24],

$$\rho = \frac{1}{4}\Big[I_A \otimes I_B + I_A \otimes (\vec{r}\cdot\vec{\sigma}^B) + (\vec{s}\cdot\vec{\sigma}^A)\otimes I_B + \sum_{i,j=x,y,z} c_{ij}\sigma_i^A \otimes \sigma_j^B\Big], \tag{1}$$

where the polarization vectors are $\vec{r} = \mathrm{tr}[\rho(I_A \otimes \vec{\sigma}^B)]$ and $\vec{s} = \mathrm{tr}[\rho(\vec{\sigma}^A \otimes I_B)]$, the elements of the correlation matrix C are $c_{ij} = \mathrm{tr}[\rho(\vec{\sigma_i}^A \otimes \vec{\sigma_j}^B)]$, the indices A and B refer to the first and second subsystems, and $i, j = x, y, z$ refer to the indices of a vector of Pauli matrices, namely $\{\sigma_x, \sigma_y, \sigma_z\}$.

It is simple to define the quantum correlations used throughout this work (Bell's nonlocality, entanglement, quantum discord, and coherence) using this representation.

Bell's nonlocality. Bell's inequality can be evaluated by the quantity [25]

$$B(\rho) = 2\sqrt{m_1 + m_2}, \tag{2}$$

where m_1 and m_2 are the two largest eigenvalues of the matrix $\mathcal{M} = CC^T$, where T means the transposition operation. If $B(\rho) \leqslant 2$, Bell's inequality is not violated, otherwise nonlocal effects might appear. The values of $B(\rho)$ are comprised in the interval $[0, 2\sqrt{2}]$, with the maximum violation being achieved by the entangled pure states, such as the Bell entangled states.

Entanglement. To quantify bipartite entanglement, we used *Negativity* [26] defined as

$$N(\rho) = \frac{\|\rho^{T_A}\|_1 - 1}{2}, \tag{3}$$

where T_A is the partial transposition of the subsystem A, and $\|\cdot\|_1$ is the trace norm. The negativity indicates how far the partial trace of the density matrix is from positive, and consequently, how entangled the subsystems are. For a two-qubit system, $N(\rho) \in [0, 1/2]$.

Quantum discord. The geometric discord of an arbitrary two-qubit state is [8]

$$D(\rho) = \tfrac{1}{4}\big(\|\vec{s}\|_2^2 + \|C\|_2^2 - \lambda_{\max}\big), \tag{4}$$

where the norms on the right-hand side of the equation above have been calculated using the Euclidean (for vector $\vec{s}$) and Hilbert-Schmidt (for matrix C) norms. $\lambda_{\max}$ represents the largest eigenvalue of the matrix

$$\Lambda = \vec{s}\cdot\vec{s}^T + CC^T.$$

The values of quantum discord are restricted to the interval $D(\rho) \in [0, 1/2]$.

Coherence. The trace norm coherence is measured using [27,28]

$$C(\rho) = \|\rho - \rho_{\mathrm{diag}}\|_1, \tag{5}$$

where ρ_{diag} denotes the state obtained from ρ using just the diagonal elements. Basically, this measure sums the absolute values of all off-diagonal terms of ρ so that $C(\rho) \in [0, 3]$ for a two-qubit system.

To explore the quantum correlations presented in the output states of the DQC1 circuit for two qubits (see Fig. 1), we chose 10^6 random initial qubit states according to the Hilbert-Schmidt measure [29] and also 10^6 unitary matrices (U_1) from the Haar measure [30,31]. The quantum correlations generated between the two qubits at the end of the circuit are shown in Fig. 2, where each dot is obtained for a given final density matrix.

As is already known, there is no entanglement between the control and the auxiliary qubits in the standard DQC1 model [4], and a straightforward consequence of this is no violation of Bell's inequality, as shown in Figs. 2(a) and 2(b). Superposition (quantified by coherence) is vital for the appearance of others correlations, as shown in Figs. 2(a) and 2(c). We also have Fig. 2(c) showing states with nonvanishing quantum discord $D(\rho)$ and coherence, confirming that they are intimately related. Note the maximum values achieved by coherence and quantum discord, $C_{\max}(\rho) = 1$ and $D_{\max}(\rho) = 0.1244$, respectively. They are far from reaching the maximum values accessible for general two-qubit states, i.e., 3 and 0.5, respectively.

III. POSTSELECTION IN THE DQC1 MODEL

Inspired by Ref. [13], we analyzed the effect of postselection on promoting quantum correlations in the DQC1 model for two qubits.

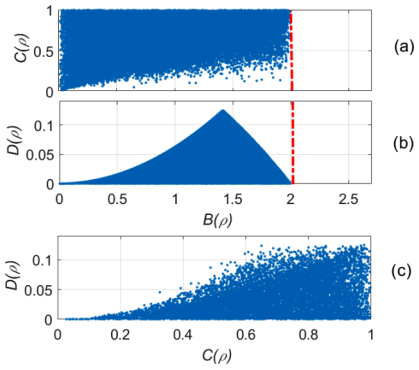

FIG. 2. Each dot represents the value of the quantum correlation calculated for the output state of the DQC1 circuit. The 10^6 states were obtained choosing initial states and unitary transformations at random. The red-dashed vertical line represents the maximum value of $B(\rho)$ in which there is no Bell's nonlocality. The quantum correlation measured by entanglement does not appear here because it is null for the standard DQC1 circuit (see Fig. 1).

To promote other correlations in this computing model, we introduced a specific postselection process F on the control qubit at the end of the DQC1 circuit (see Fig. 3), which one enacts through a local filter, described by [32]

$$F(U_a, \eta) = U_a \begin{bmatrix} 1 & 0 \\ 0 & \eta \end{bmatrix} U_a^\dagger, \tag{6}$$

with $\eta \in [0, 1]$, and U_a is a unitary matrix. η represents the probability of success of this filter considering the complete measurement $\{F(U_a, \eta), I - F(U_a, \eta)\}$. For the particular case $\eta = 1$, the filter reduces to the identity operator, doing nothing on the control qubit, while for $\eta < 1$, it diminishes the contribution coming from one component of the state in the direction determined by the unitary transformation U_a. In the limit case $\eta = 0$, just one component of the state survives.

As is well known, if the auxiliary qubit starts in a state different from the maximum mixture, then, for an appropriate unitary U_1, entanglement and violation of Bell's inequality emerge in this system [33]. Thus, in order to purify the auxiliary qubit, we postselect certain values of η and investigate the role played by this filter parameter on the quantum correlations between the qubits.

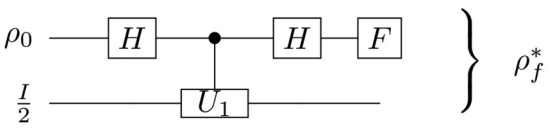

FIG. 3. DQC1 model for two qubits with postselection through a specific filter F that operates on the control qubit. The initial state of the auxiliary qubit is $\rho_{n=1} = \frac{I}{2}$, while the initial state of the control qubit ρ_0 and the unitary U_1 are randomly chosen. At the end of the circuit, we trace out the control qubit from the two-qubit state ρ_f^*, obtaining a more purified state of the auxiliary qubit. The purification process can be repeated by inserting the final state of the auxiliary qubit in the circuit again as many times as desired.

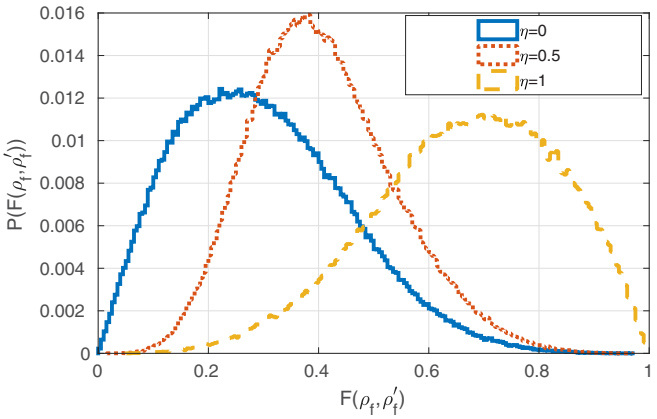

FIG. 4. Empirical probability distribution of the fidelity between 10^4 randomly chosen ρ_f and ρ_f' after the DQC1 with postselection [see Eq. (8)] for fixed values of $\eta \in \{0, 1/2, 1\}$.

A. Benchmarking the DQC1 with postselection

To proceed with this investigation, we used a DQC1 with postselection; see Fig. 3. The state before filtering is

$$\rho_{bf} = (H \otimes I)U(H \otimes I)\rho_0(H \otimes I)U^\dagger(H \otimes I), \tag{7}$$

and the final state is

$$\rho_f(U_a, \eta) = \frac{F(U_a, \eta)\rho_{bf}F(U_a, \eta)^\dagger}{\mathrm{tr}[F(U_a, \eta)\rho_{bf}F(U_a, \eta)^\dagger]} \tag{8}$$

for some choice of $\eta \in [0, 1]$ and unitary matrix U_a.

Following [34], we first analyze the fidelity,

$$F(\rho_1, \rho_2) = \left[\sqrt{\sqrt{\rho_1}\rho_2\sqrt{\rho_1}}\right]^2,$$

between 10^4 pairs of output states ρ_f and ρ_f' choosing an initial pure state ρ_0 for the control qubit drawn from the Hilbert-Schmidt measure, a controlled unitary gate U_1, and a unitary U_a drawn from Haar measure and fixed values of $\eta \in \{0, 1/2, 1\}$.

The probability distributions of $F(\rho_f, \rho_f')$ in Fig. 4 show the average fidelity between ρ_f and ρ_f' diminishing as $\eta \to 0$. We can see it as numerical evidence that the DQC1 with postselection distributes the states more distantly (according to the Bures metric [35]), and also with more accessible states in the two-qubit Hilbert space, which will be clear when we present the promotion of quantum correlations later in this article.

To understand this result qualitatively, let us remember that the motivation of the DQC1 model relies on nuclear magnetic resonance (NMR) systems, whose two-qubit density matrices have the form

$$\rho_{\mathrm{NMR}} = \frac{1 - \epsilon}{4} I_{4\times4} + \epsilon|\psi\rangle\langle\psi|, \tag{9}$$

with $0 \leqslant \epsilon \leqslant 1$, and $I_{4\times4}$ and $|\psi\rangle$ are the identity operator and a pure state in the two-qubit Hilbert space. If we calculate the fidelity for states of the form ρ_{NMR}, it is easy to verify that for small values of ϵ, states with fidelities closer to 1 are more frequent, which is similar to the standard DQC1 model.

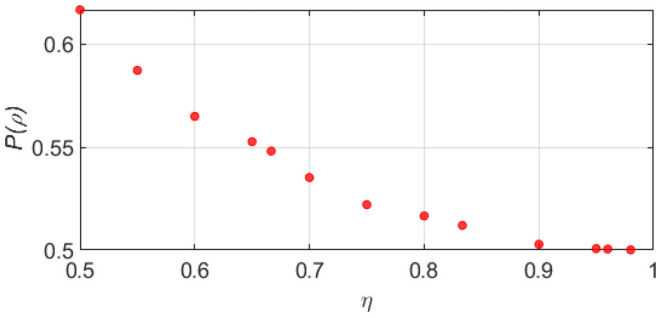

FIG. 5. Purity as a function of the probability of success η for the DQC1 model with two qubits and postselection. Each dot represents the average maximum value of the achieved purity for the auxiliary qubit with a specific η.

B. Purity and quantum correlations in the DQC1 model

As mentioned before, the purity $P(\rho) = \mathrm{tr}\rho^2$ of the auxiliary qubit also determines the possibility of promoting quantum correlations in the DQC1 model. The purity varies from $P(\rho) = 1/2$ for a totally mixed qubit state to $P(\rho) = 1$ for a pure qubit state. In Fig. 5 we run the same protocol above and take the average maximum value of the purity for a specific value of η. We observe that the average maximum value of the purity is approximately $P(\rho) \simeq 0.62$ for $\eta = 0.5$, and as η approaches 1 the purity converges to its minimum value, as expected, since for $\eta = 1$ the filter has no effect on the auxiliary qubit.

Figure 6 shows the behavior of each normalized quantum correlation as a function of the purity of the auxiliary qubit. The normalization of a given quantum correlation X is defined as $X_N \equiv X/X_{\max}$, where $X_{\max}$ is the maximum value achieved by the quantum correlation X. All correlations increase as the purity increases. We highlight that even without a significant purification of the auxiliary qubit, we already achieve non-null entanglement and Bell's nonlocality [$B_N(\rho) > 1/\sqrt{2} \simeq 0.707$]. These results are in agreement with the discussion made in the previous section in which coherence (blue disks) and quantum discord (yellow diamonds) exist independently of the purification process, once they are created by local operations (and classical communications for discord). On the other hand, the existence of entanglement (red squares)

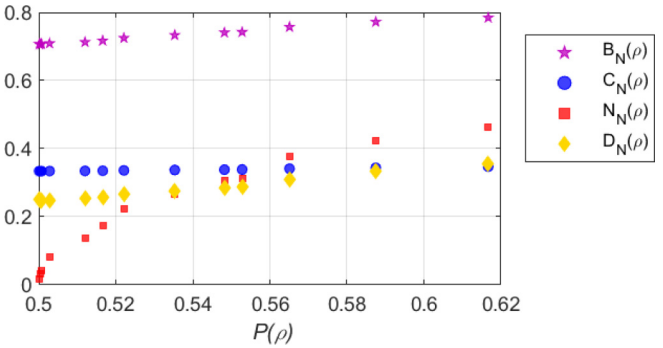

FIG. 6. Normalized quantum correlations as a function of purity $P(\rho)$. Each dot represents the average maximum value of the quantum correlations for a given purity.

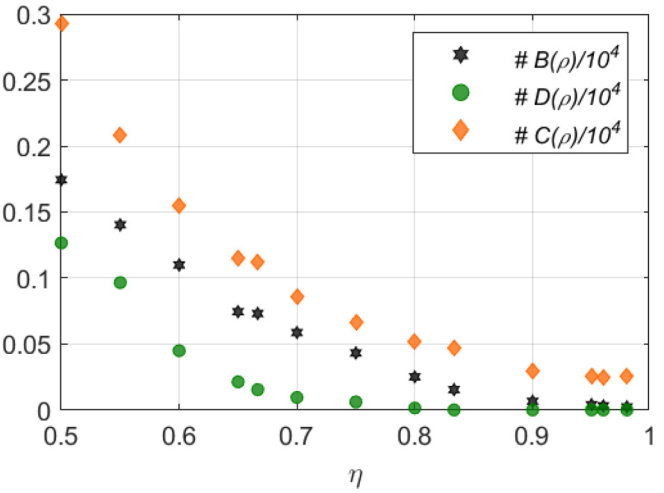

FIG. 7. Density of states, defined as the ratio between the number of states after the postselection process with a correlation value greater than the maximum value of the correlation achieved by the states in the standard DQC1 model (without postselection), vs the probability of success η of the purification protocol. The total number of states analyzed for each correlation is 10^4.

and Bell's nonlocality (pink stars) depends strongly on the purity of the auxiliary qubit. Entanglement starts from zero for totally mixed states [$P(\rho) = 1/2$] and increases, but it does not achieve maximum entanglement. A similar behavior is found for the violation of Bell's inequality, although its minimum value is greater than $1/\sqrt{2}$.

To estimate the number of states that have been promoted after the postselection process, i.e., the number of states whose quantum correlations increased after the filtering procedure, we analyze the density of states. The density of states is defined as the ratio between the number of states after the postselection process with a correlation value greater than the maximum value of the correlation achieved by the states in the standard DQC1 model (without postselection). The maximum values of quantum discord, quantum coherence, and $B(\rho)$ attained by the standard DQC1 circuit (see Fig. 2) are 0.1244, 0.9992, and 1.9974, respectively. Figure 7 presents the density of states for quantum discord (green disks), quantum coherence (orange diamonds), and $B(\rho)$ (black stars) for the different values of η considering a total of 10^4 states. As there is no entanglement between the control and the auxiliary qubit in the standard DQC1 model, the density of states defined above does not apply for this correlation. We observe that the higher η is, the lower is the density of states that overcome the value of these correlations for the DQC1 model without postselection. This reinforces the strong connection between the mixedness of the auxiliary qubits and the quantum correlations in the model. As in the standard DQC1 model, the maximum value achieved by $B(\rho)$ is approximately 2; all states used to build Fig. 7 (black stars) violate Bell's inequality. These plots give us information about the number of states that are accessible after the postselection process, and which ones constitute a resource for quantum computation.

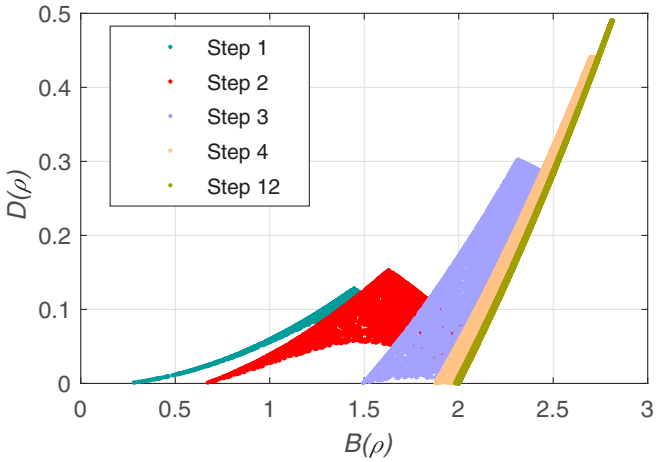

FIG. 8. Quantum discord $D(\rho)$ vs $B(\rho)$. Each surface with a different color shows the mean value of 10^4 random unitary matrices U_1 and control qubit initial states used to compute the quantum correlations for each purification step of the auxiliary qubit. Due to the similar behavior of the quantum correlations for the intermediate steps of the purification process, only 5 out of a total of 12 steps have been plotted.

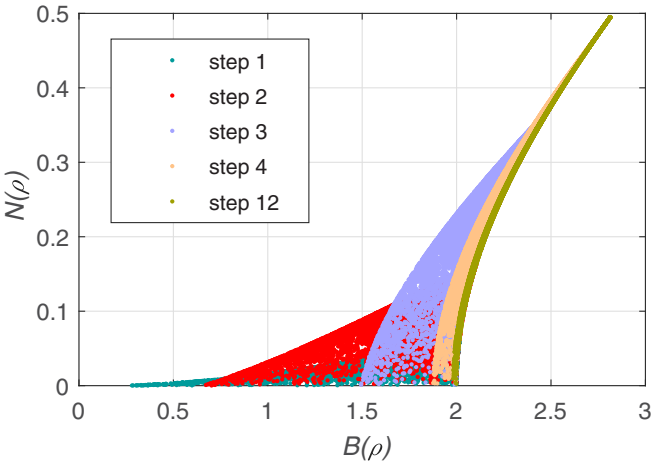

FIG. 9. Negativity $N(\rho)$ vs $B(\rho)$. Each surface with a different color shows the mean value of 10^4 random unitary matrices U_1 and control qubit initial states used to compute the quantum correlations for each purification step of the auxiliary qubit. Due to the similar behavior of the quantum correlations for the intermediate steps of the purification process, only 5 out of a total of 12 steps have been plotted.

C. Purification optimization

Now we want to find optimal strategies for filtering, without fixing the parameter η, to reach a purity of $P(\rho) = 0.99$ for the auxiliary system.

For this optimization, we chose the following procedure:

(i) The initial pure state ρ_0 for the control qubit and the controlled unitary gate U_1 are drawn from Hilbert-Schmidt and Haar measures, respectively.

(ii) The parameters of the filter F, which include η and the unitary U_a, are chosen such that

$$\arg \min_{\eta, U_a} \{P(\mathrm{tr}_c[\rho_f(U_a, \eta)])\},$$

where $\mathrm{tr}_c[\rho_f(U_a, \eta)]$ is the state of the auxiliary system after the postselection, tracing the control system out.

(iii) If $P(\mathrm{tr}_c[\rho_f(U_a, \eta)]) \approx 0.99$ we stop.

(iv) Otherwise, the purified state of the auxiliary qubit is chosen in the DQC1 circuit instead of the identity, and we optimize again for the same choice of initial pure state ρ_0 for the control qubit and the controlled unitary gate U_1.

We noticed that on average 12 steps were necessary to achieve the desired value of purity. The relation between the quantum correlations with the steps of purification are shown in Figs. 8–13. Each surface with a different color shows the mean value of 10^4 random unitary matrices U_1 and initial states of the control qubit used to compute the quantum correlations for each purification step of the auxiliary qubit. To keep the figures legible, we have plotted only 5 steps out of a total of 12, i.e., the 1st, 2nd, 3rd, 4th, and 12th ones. The teal surfaces represent the mean value of quantum correlations after the first step of purification, while the olive surfaces represent the mean value after the last step of purification, in which the auxiliary qubit achieves $P(\rho) = 0.99$.

Figures 8–10 show that according to the increase of the purity of the auxiliary qubit, the number of states that violate Bell's inequality also increases, almost achieving its maximum violation. From step three onward, the quantum correlations behave totally differently. In Fig. 10, we clearly see that Bell's inequality is violated already in the second step of purification, and from the fourth step onward almost all of the states are nonlocal. Also, Figs. 8 and 9 agree for highly purified auxiliary states once quantum discord and entanglement quantify the same kind of correlation [8]. In Fig. 10, we observe that in all steps of purification of the auxiliary qubit,

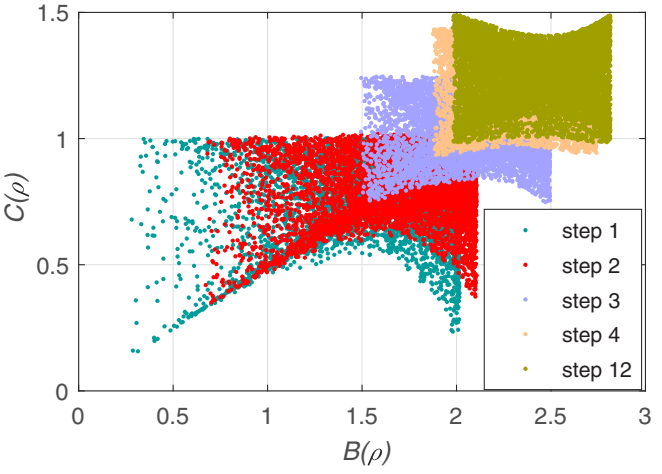

FIG. 10. Quantum coherence $C(\rho)$ vs $B(\rho)$. Each surface with a different color shows the mean value of 10^4 random unitary matrices U_1 and control qubit initial states used to compute the quantum correlations for each purification step of the auxiliary qubit. Due to the similar behavior of the quantum correlations for the intermediate steps of the purification process, only 5 out of a total of 12 steps have been plotted.

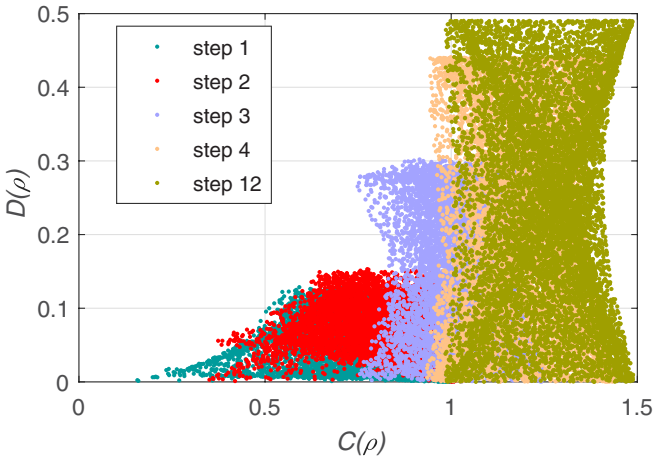

FIG. 11. Quantum discord $D(\rho)$ vs quantum coherence $C(\rho)$. Each surface with a different color shows the mean value of 10^4 random unitary matrices U_1 and control qubit initial states used to compute the quantum correlations for each purification step of the auxiliary qubit. Due to the similar behavior of the quantum correlations for the intermediate steps of the purification process, only 5 out of a total of 12 steps have been plotted.

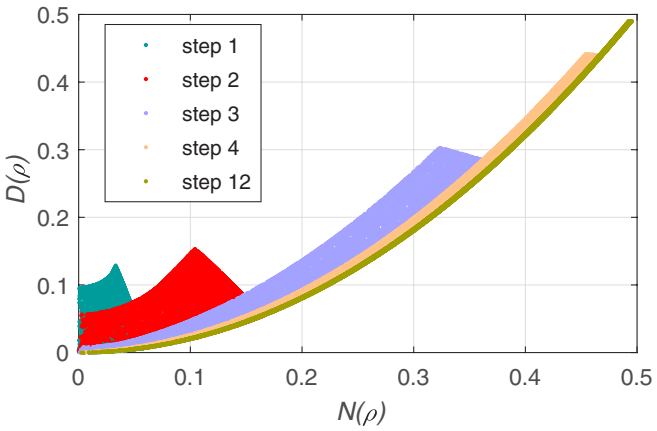

FIG. 13. Quantum discord $D(\rho)$ vs negativity $N(\rho)$. Each surface with a different color shows the mean value of 10^4 random unitary matrices U_1 and control qubit initial states used to compute the quantum correlations for each purification step of the auxiliary qubit. Due to the similar behavior of the quantum correlations for the intermediate steps of the purification process, only 5 out of a total of 12 steps have been plotted.

the states have non-null coherence, achieving a maximum value of approximately 1.5. Such a value is also achieved by states that violate almost maximally Bell's inequality, i.e., they are of the form $\frac{|00\rangle+|11\rangle}{\sqrt{2}}$, which gives us a coherence value of $\sqrt{2} \simeq 1.41$. Figures 11 and 12 show that for the last step of purification, almost all of the states have $C(\rho) > 1$, which demonstrates the efficiency of the purification protocol.

The general behavior of quantum correlations presented in Fig. 13 agrees with the result presented in Refs. [36,37], which states that when using 2-norm, quantum discord is lower bounded by the square of the negativity for two qubit states.

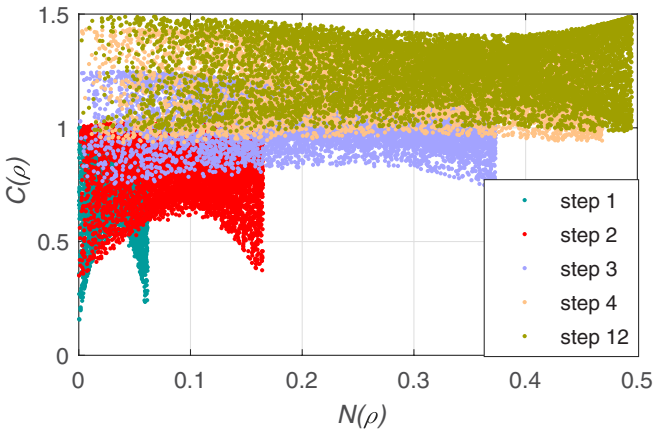

FIG. 12. Quantum coherence $C(\rho)$ vs negativity $N(\rho)$. Each surface with a different color shows the mean value of 10^4 random unitary matrices U_1 and control qubit initial states used to compute the quantum correlations for each purification step of the auxiliary qubit. Due to the similar behavior of the quantum correlations for the intermediate steps of the purification process, only 5 out of a total of 12 steps have been plotted.

As mentioned above, for entangled states that are almost pure, both measures become quite similar.

IV. CONCLUSIONS

In this work, we showed how to promote quantum correlations, such as coherence, quantum discord, entanglement, and Bell's nonlocality, that are present in the output state of the DQC1 model for two qubits. As is already known, in the standard DQC1 model for two qubits there is only quantum discord and coherence. By applying a filtering process combined with optimization protocols, entanglement and Bell's nonlocality arise in this system, even for a small purification of the auxiliary qubit. When we reintroduced the purified auxiliary qubit into the circuit again, we observed that the number of purification steps that are needed to achieve a maximum purity of 0.99 is on average 12. For this level of purity, the qubits become practically maximally entangled, and they also violate Bell's inequality almost maximally. Our results suggest that it is possible to promote this restricted model of quantum computing to a universal one by using postselection with a specific filter, although formal proof is lacking. A rather natural extension of our analysis is to consider the effect of decoherence and/or dissipation in the scheme presented. This will be done in a future work.

ACKNOWLEDGMENTS

The authors thank Ana Sprotte, Ernesto Galvão, and Susane Caligari for useful discussions. The authors also acknowledge the financial support from the Brazilian funding agencies CNPq, CAPES, and the National Institute for Science and Technology of Quantum Information (INCT/IQ).

[1] R. Jozsa and N. Linden, Proc. R. Soc. London, Ser. A **459**, 2011 (2003).
[2] M. Van den Nest, Phys. Rev. Lett. **110**, 060504 (2013).
[3] E. Knill and R. Laflamme, Phys. Rev. Lett. **81**, 5672 (1998).
[4] A. Datta, S. T. Flammia, and C. M. Caves, Phys. Rev. A **72**, 042316 (2005).
[5] A. Datta and G. Vidal, Phys. Rev. A **75**, 042310 (2007).
[6] A. Datta, A. Shaji, and C. M. Caves, Phys. Rev. Lett. **100**, 050502 (2008).
[7] A. Ferraro, L. Aolita, D. Cavalcanti, F. M. Cucchietti, and A. Acín, Phys. Rev. A **81**, 052318 (2010).
[8] B. Dakić, V. Vedral, and Č. Brukner, Phys. Rev. Lett. **105**, 190502 (2010).
[9] J. Ma, B. Yadin, D. Girolami, V. Vedral, and M. Gu, Phys. Rev. Lett. **116**, 160407 (2016).
[10] J. M. Matera, D. Egloff, N. Killoran, and M. B. Plenio, Quantum Sci. Technol. **1**, 01LT01 (2016).
[11] A. Datta, Ph.D. thesis, University of New Mexico, 2008, arXiv:0807.4490.
[12] D. Poulin, R. Laflamme, G. J. Milburn, and J. P. Paz, Phys. Rev. A **68**, 022302 (2003).
[13] S. Parker and M. B. Plenio, Phys. Rev. Lett. **85**, 3049 (2000).
[14] D. Poulin, R. Blume-Kohout, R. Laflamme, and H. Ollivier, Phys. Rev. Lett. **92**, 177906 (2004).
[15] P. W. Shor and S. P. Jordan, Quantum Inf. Comput. **8**, 681 (2008).
[16] S. Boixo and R. D. Somma, Phys. Rev. A **77**, 052320 (2008).
[17] H. Cable, M. Gu, and K. Modi, Phys. Rev. A **93**, 040304(R) (2016).
[18] B. P. Lanyon, M. Barbieri, M. P. Almeida, and A. G. White, Phys. Rev. Lett. **101**, 200501 (2008).
[19] M. Hor-Meyll, D. S. Tasca, S. P. Walborn, P. H. Souto Ribeiro, M. M. Santos, and E. I. Duzzioni, Phys. Rev. A **92**, 012337 (2015).
[20] G. Passante, O. Moussa, C. A. Ryan, and R. Laflamme, Phys. Rev. Lett. **103**, 250501 (2009).
[21] G. Passante, O. Moussa, D. A. Trottier, and R. Laflamme, Phys. Rev. A **84**, 044302 (2011).
[22] W. Wang, J. Han, B. Yadin, Y. Ma, J. Ma, W. Cai, Y. Xu, L. Hu, H. Wang, Y. P. Song, M. Gu, and L. Sun, Phys. Rev. Lett. **123**, 220501 (2019).
[23] K. Krzyzanowska, M. Copley-May, R. Romain, C. MacCormick, and S. Bergamini, J. Phys.: Conf. Ser. **793**, 012015 (2017).
[24] U. Fano, Rev. Mod. Phys. **55**, 855 (1983).
[25] R. Horodecki, P. Horodecki, and M. Horodecki, Phys. Lett. A **200**, 340 (1995).
[26] G. Vidal and R. F. Werner, Phys. Rev. A **65**, 032314 (2002).
[27] T. Baumgratz, M. Cramer, and M. B. Plenio, Phys. Rev. Lett. **113**, 140401 (2014).
[28] X.-D. Yu, D.-J. Zhang, G. F. Xu, and D. M. Tong, Phys. Rev. A **94**, 060302(R) (2016).
[29] K. Życzkowski, K. A. Penson, I. Nechita, and B. Collins, J. Math. Phys. **52**, 062201 (2011).
[30] K. Zyczkowski and M. Kus, J. Phys. A **27**, 4235 (1994).
[31] M. Ozols (unpublished)
[32] A. Kent, N. Linden, and S. Massar, Phys. Rev. Lett. **83**, 2656 (1999).
[33] M. Piani, S. Gharibian, G. Adesso, J. Calsamiglia, P. Horodecki, and A. Winter, Phys. Rev. Lett. **106**, 220403 (2011).
[34] K. Życzkowski and H.-J. Sommers, Phys. Rev. A **71**, 032313 (2005).
[35] W. K. Wootters, Phys. Rev. D **23**, 357 (1981).
[36] T. Debarba, T. O. Maciel, and R. O. Vianna, Phys. Rev. A **86**, 024302 (2012).
[37] D. Girolami and G. Adesso, Phys. Rev. A **84**, 052110 (2011).